ISSN 0915-6364

NATIONAL INSTITUTE FOR FUSION SCIENCE

Low Energy Electron Capture in Collisions of C^{3+} with He

Y. Wu, Y.Y.Qi, J. Yan, J.G. Wang, Y. Li, R.J. Buenker and D. Kato

(Received - Apr. 13, 2009)

NIFS-DATA-106 June 18, 2009

RESEARCH REPORT
NIFS-DATA Series

TOKI, JAPAN

Low energy electron capture in collisions of C^{3+} with He

Y. Wu[1], Y.Y.Qi [1,2], J. Yan[1], J. G. Wang [1],Y. Li[3]， R. J. Buenker[3] and D. Kato[4]

[1] *Institute of Applied Physics and Computational Mathematics, PO Box 8009, Beijing 100088, China*
[2]*School of Electrical Engineering, Jiaxing University, Jiaxing 314001, China*
[3]*Fachbereich C-Mathematik und Naturwissenschaften,*
Bergische Universität Wuppertal, D-42097 Wuppertal, Germany
[4]*Natinal Institute for Fusion Science, Toki 509-5292, Japan*

Charge transfer processes due to collisions of ground state $C^{3+}(1s^22s\ ^2S)$ ions with He atom are investigated using the quantum-mechanical molecular-orbital close-coupling (QMOCC) method for energies between 10^{-4}eV/u and 10^3eV/u. The *ab initio* adiabatic potential and radial coupling utilized in the QMOCC calculations are obtained from the multi-reference single- and double-excitation configuration interaction (MRD-CI) approach. Total and state-selective single electron capture (SEC) cross sections and rate coefficients are obtained and compared with the available experimental and theoretical data. Good agreement between the measured SEC cross sections and the present calculation is found, but the previous calculation of total rate coefficient using the Landau–Zener model is one or two orders of magnitude smaller than the present result.

Keywords: ion-atom collision, molecular-orbital close-coupling method, state-selective single electron capture, multi-reference single- and double-excitation configuration interaction

I. INTRODUCTION

Charge transfer process at low collision energies has attracted much attention because of their importance not only in basic atomic physics but also in various application fields due to the typically large electron-capture cross sections. For example, in X-ray ionized astronomical environments, charge transfer provides a recombination mechanism for multiply charged ions [1]. In a core of Tokamak plasma, charge exchange spectrum produced by neutral beam injection is an important method for diagnosing the abundances of impurities. In the Tokamak diverter, charge exchange of impurity ions with neutral atoms and molecules plays an important role in the plasma ionization balance and the radiative energy loss leading to cooling [2,3]. Carbon is one of the major impurities in the magnetic confinement fusion devices and helium is the product in the fusion reaction, so the charge transfer between multicharged carbon and helium is important for simulation and diagnostics in Tokamak plasma.

For the low-energy electron capture process in collisions of C^{3+} with He, several groups have reported their measurements [4-7]. Lennon et al. [5] and Kimura et al. [6] utilized the translational energy-gain spectroscopy technique to measure the total and state-selective single-electron capture cross sections for a few energies from 250eV/u to 1500eV/u. Iwai et al. [4] have also measured the total single charge cross section for several energy points of 375eV/u, 500eV/u and 625eV/u. Recently, Ishii et al. measured the charge transfer cross section for a broad range of collision energies between 0.3eV and 5.4KeV [7] by employing an octupole ion beam guide and the mini-EBIS (electron beam ions source) apparatus, and they also estimated the single- and double-charge cross sections using the Classical overbarrier (COB) and Multichannel Landau-Zener (MCLZ) methods. Butler and Dalgarno [8] have done the Landau-Zener calculation in the thermal energy region. As our knowledge, no *ab initio* quantal calculation has been done

for this system.

In the present work, the charge transfer process due to collisions of ground state $C^{3+}(1s^2 2s\ \ ^2S)$ ions with helium atom is studied using the quantum-mechanical MOCC method. The adiabatic potential curves and radial coupling matrix elements are calculated with an *ab. initio* multireference configuration interaction (MRD-CI) package [9-11]. Total and state-selective cross sections are obtained and compared with the available theoretical and experimental data. Sect. II describes the electronic structure calculation of $[CHe]^{3+}$, while Sect. III introduces the scattering calculation briefly. Sect. IV presents the obtained potentials and couplings as well as the results of the scattering calculations including comparisons with other theoretical calculations and experiments, while Sect. V briefly gives a summary of the work. Atomic units are used throughout unless otherwise noted.

II. THEORETICAL METHOD

A. Electronic Structure Calculation

In the present work, the adiabatic potential curves of $^2\Sigma^+$ electronic states in A_1 symmetry of $[CHe]^{3+}$ system are obtained by employing the *ab initio* multireference single- and double-excitation configuration interaction (MRD-CI) method [9-11], with an individual configuration selection for each state under consideration and subsequent energy extrapolation, using the Table CI algorithm [10]. All electrons are considered explicitly. A correlation consistent basis set (6s, 2p, 1d) contracted to [3s, 2p, 1d] basis set [12] is employed for helium, and a correlation consistent basis set (23s, 8p, 5d, 2f) contracted to [7s, 6p, 5d, 2f] basis set [13] is employed for carbon. In addition, two *s*-type, two *p*-type and two *d*-type diffuse functions for C atom have been added to the above basis set to describe the Rydberg states, while one *s*-type, one *p*-type and one *d*-type diffuse functions have been used for the He atom. Therefore, the final basis set for the helium atom is (7s, 3p, 2d) contracted to [4s, 3p, 2d] and for the carbon atom is (25s, 10p, 7d, 4f) contracted to [9s, 8p, 7d, 4f]. All the diffuse basis sets are optimized and the asymptotic excitation energies obtained are accurate within 1% compared with the corresponding NIST atomic and spectroscopic data tables [14]. A threshold value of 1.0×10^{-9} Hartree is employed to select the configuration wave functions for $[CHe]^{3+}$ internuclear distances in the region of 1.0 to 50 a_0, i.e., each configuration generated by single or double excitation from a reference set is checked, whether its energy lowering is equal to or greater than *T* (then it is included in the first set of configurations) or less than *T* (then it is discarded, but its lowering contribution is summed up for the extrapolation step). The total numbers of the selected configuration functions are dependent on the internuclear distances and generally the total numbers are less than 40000. The energy lowering contributed from the unselected configuration functions is considered by employing an extrapolation procedure [9, 10]. As shown in table 1, the errors in calculated energy positions for the computed electronic states fall in the 0.07 eV range in the asymptotic region, which is adequate for most scattering calculations [15]. The adiabatic radial coupling elements are calculated by using a finite-difference method [16] and this is done using the actually determined wave functions without any extrapolation. The adiabatic potentials and radial couplings for the initial $[C^{3+} + He]$ state and charge-transfer channels lying close to the initial channels have been computed and will be presented in section IV.

Table 1. Comparison of dissociation energies of the $[CHe]^{3+}$ system between the present MRDCI calculation and the corresponding experimental data [17] ; ΔE is the absolute error between the calculated and experimental data.

Molecular states	MRDCI results (eV)	Experimental values (eV) [17]	ΔE (eV)
$1\ ^2\Sigma^+[C^{2+}(1s^22s^2\ ^1S)+He^+(1s\ ^2S)]$	0.0	0.0	0.0
$2\ ^2\Sigma^+[C^{2+}(\ 1s^22s2p\ ^3P^o)+He^+\ (1s\ ^2S)]$	6.48373	6.49563	0.01189
$3\ ^2\Sigma^+[C^{2+}(1s^22s2p\ ^1P^o)+He^+\ (1s\ ^2S)]$	12.73865	12.69004	0.04861
$4\ ^2\Sigma^+[C^{2+}(1s^22p^2\ ^1D)+He^+\ (1s\ ^2S)]$	18.10711	18.08633	0.02078
$5\ ^2\Sigma^+[C^{2+}(\ 1s^22p^2\ ^1S)+He^+\ (1s\ ^2S)]$	22.69639	22.62958	0.06681
$6\ ^2\Sigma^+[C^{3+}(1s^22s\ ^2S)+He(1s^2\ ^1S)]$	23.29427	23.30039	0.00612
$7\ ^2\Sigma^+[C^{2+}(\ 1s^22s3s\ ^3S)+He^+\ (1s\ ^2S)]$	29.49488	29.53465	0.03976
$8\ ^2\Sigma^+[C^+(1s^22s^22P\ ^2P^o)+He^{2+}]$	30.08816	30.03445	0.0537

B. Scattering Method

The MOCC method, which we only briefly discuss here, has been described thoroughly in the literature (e.g. Kimura and Lane [18], Zygelman et al. [19], Wang et al. [20]). It involves solving a coupled set of second-order differential equations using the log-derivative method of Johnson [21]. In the adiabatic representation, transitions between channels are driven by radial and rotational matrix elements of the vector potential $\underline{A}(\vec{R})$, where $\vec{R}$ is the internuclear distance vector. Since the adiabatic description contains first-order derivatives, it is numerically convenient to make a unitary transformation [19, 22,23], which is dependent on the radial portion of $\underline{A}(\vec{R})$, to a diabatic representation

$$\underline{U}(R) = \underline{W}(R)\ [\underline{V}(R) - \underline{P}(R)]\ \underline{W}^{-1}(R) \qquad (1)$$

where $\underline{U}(R)$ is the diabatic potential matrix, $\underline{V}(R)$ is the diagonal adiabatic potential, $\underline{W}(R)$ is a unitary transformation matrix, and $\underline{P}(R)$ is the rotational matrix of the vector potential $\underline{A}(\vec{R})$ [20,24,25]. In this work, the rotational couplings are neglected, since the radial couplings should be the dominant mechanism for charge transfer in the calculated energy region (~0.1eV/u-10^3eV/u) [20, 26, 27]. With the diabatic potentials and couplings, the coupled set of second-order differential equations is solved to obtain the *K*-matrix from the scattering amplitude after a partial-wave decomposition (see e.g. Zygelman et al. [19]). The electron capture cross section is then given by

$$\sigma_{\alpha\to\beta} = \frac{\pi g_\alpha}{k_\alpha^2}\sum_J (2J+1)\left|(S_J)_{\alpha\beta}\right|^2, \qquad (2)$$

where the *S*-matrix is defined as

$$\underline{S}_J = [\underline{I} + i\underline{K}_J]^{-1}\ [\underline{I} - i\underline{K}_J] \qquad (3)$$

$\underline{I}$ is the identity matrix, k_α denotes the wave number for center-of-mass motion of the initial ion-atom channel and g_α is an approach probability factor of the initial channel α. Electron translation factors (ETF's) [18] are not included in the current calculations, since the influence of ETF's is only expected to be important when the incident energy $E > 1keV/u$ [20, 28, 29]. The method described above is carried out for each partial wave until a converged cross section is attained.

III. RESULTS AND DISCUSSION

In the present MOCC calculations, only the radial couplings are considered and the rotational couplings are neglected. Since the symmetries of the entrance channels of $C^{3+}(2s^2 2p\ ^2P^o)$ + $He(1s^2\ ^1S)$ are exclusively $^2\Sigma^+$, we only treat exit channels of this symmetry. It can be found from Table 1 that the energy intervals between the initial channel and the first and second endoergic channels, namely 7 $^2\Sigma^+$ ($C^{2+}(1s^2 2s3s\ ^3S)+He^+$ ($1s\ ^2S$)) and 8 $^2\Sigma^+$ ($C^+(1s^2 2s^2 2P\ ^2P^o)+He^{2+}$) are as large as ~ 6.2eV and ~7.0eV respectively, so that the endoergic states should be not important for charge transfer processes in the concerned energy region (10^{-4} eV/u ~ 10^3 eV/u). The second endoergic channel is a double charge transfer channel, therefore the double electron capture process is expected to be negligible in the energy region considered. Six lowest $^2\Sigma^+$ channels have been considered in the present work, that is, $C^{2+}(1s^2 2s^2\ ^1S)+He^+(1s\ ^2S)(1\ ^2\Sigma^+)$, $C^{2+}(1s^2 2s2p\ ^3P^o)+He^+(1s\ ^2S)(2\ ^2\Sigma^+)$, $C^{2+}(1s^2 2s2p\ ^1P^o)+He^+(1s\ ^2S)(3\ ^2\Sigma^+)$, $C^{2+}(1s^2 2p^2\ ^1D)+He^+$ ($1s\ ^2S$) ($4\ ^2\Sigma^+$), $C^{2+}(1s^2 2p^2\ ^1S)+He^+$ ($1s\ ^2S$) ($5\ ^2\Sigma^+$), $C^{3+}(1s^2 2s\ ^2S)+He(1s^2\ ^1S)$ ($6\ ^2\Sigma^+$), in which the $6^2\Sigma^+$ corresponds to the incident channel.

A. **Potentials and Radial Couplings**

For the six $^2\Sigma^+$ states included in the MOCC calculations, adiabatic potentials are plotted in Fig. 1 with the corresponding diabatic potentials, and the adiabatic radial couplings are shown in Fig.2. Using Eq. (1), the adiabatic potentials and couplings are transformed to the diabatic representation [20, 21].

Fig. 1 displays the adiabatic and diabatic potentials of $[CHe]^{3+}$ ($^2\Sigma^+$) as a function of internuclear distance, in which these six $^2\Sigma^+$ states correspond to $C^{2+}(1s^2 2s^2\ ^1S)+He^+(1s\ ^2S)(1\ ^2\Sigma^+)$, $C^{2+}(1s^2 2s2p\ ^3P^o)+He^+(1s\ ^2S)(2\ ^2\Sigma^+)$, $C^{2+}(1s^2 2s2p\ ^1P^o)+He^+(1s\ ^2S)(3\ ^2\Sigma^+)$, $C^{2+}(1s^2 2p^2\ ^1D)+He^+$ ($1s\ ^2S$) ($4\ ^2\Sigma^+$), $C^{2+}(1s^2 2p^2\ ^1S)+He^+$ ($1s\ ^2S$) ($5\ ^2\Sigma^+$), $C^{3+}(1s^2 2s\ ^2S)+He(1s^2\ ^1S)$ ($6\ ^2\Sigma^+$) in the asymptotic regions. Strongly avoided crossing appears around $10.5a_0$, $5.2\ a_0$ and $2.0\ a_0$ for the adiabatic potentials, which are responsible for driving the transitions between $^2\Sigma^+$ states channels. It is interesting to note that there exists an avoided crossing between $5\ ^2\Sigma^+$ and $6\ ^2\Sigma^+$ states at large internuclear distance, but that the avoided crossing distance is so large ($\sim$90 a_0) that it can be safely treated as diabatic, resulting in a negligible cross section. However, short-range avoided crossings appear between the fifth $^2\Sigma^+$ and the initial channel and other charge transfer states, and these interactions will become important at higher energies.

The adiabatic radial coupling matrix elements for $^2\Sigma^+$ states are shown in Fig.2, and only strong radial couplings between the adjacent states are presented. Each peak is consistent with the position of avoided crossing in Fig.1. It can be found that the radial couplings around $5.2\ a_0$ are much broader and smaller compared with the very sharp radial couplings at about $10.5\ a_0$, and these avoided crossings are expected to play dominant roles in the charge transfer processes. Fig. 3 plots the diabatic radial couplings of $[CHe]^{3+}$ ($^2\Sigma^+$) as a function of internuclear distance. It can be found that the couplings vary smoothly with internuclear distance R. Approaching the united-atom limit, additional avoided crossings may appear, which can result in irregular behavior and affect the high-energy charge transfer processes.

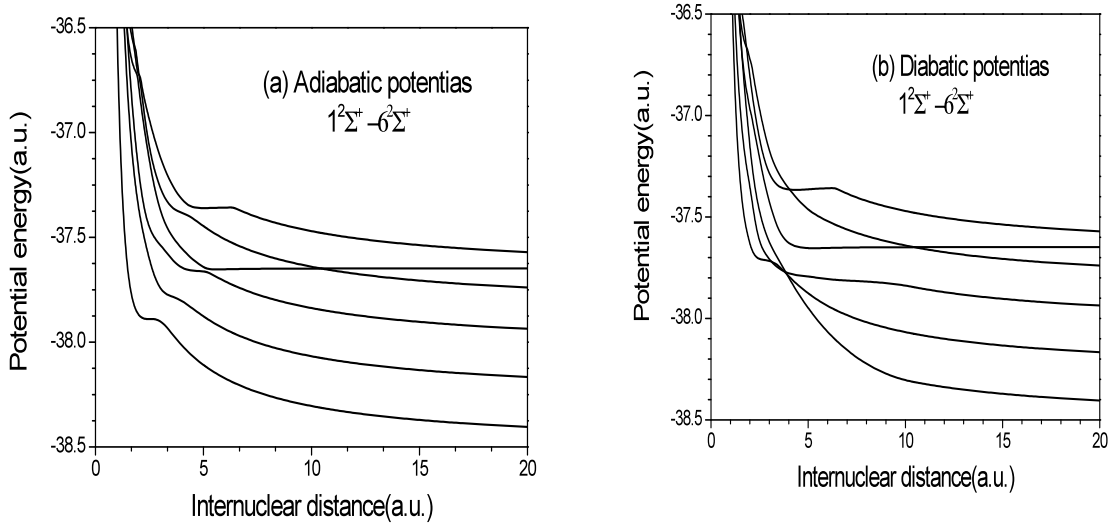

Fig. 1. Adiabatic and diabatic potentials of $[CHe]^{3+}$ $^2\Sigma^+$ states as a function of internuclear distance. Panel (a): adiabatic potentials; panel (b): diabatic potentials. The curves denote $C^{2+}(1s^22s^2\ ^1S)+He^+(1s\ ^2S)(1\ ^2\Sigma^+)$, $C^{2+}(1s^22s2p\ ^3P^o)+He^+(1s\ ^2S)(2\ ^2\Sigma^+)$, $C^{2+}(1s^22s2p\ ^1P^o)+He^+(1s\ ^2S)(3\ ^2\Sigma^+)$, $C^{2+}(1s^22p^2\ ^1D)+He^+\ (1s\ ^2S)\ (4\ ^2\Sigma^+)$, $C^{3+}(1s^22s\ ^2S)+He(1s^2\ ^1S)\ (6\ ^2\Sigma^+)$, $C^{2+}(\ 1s^22p^2\ ^1S)+He^+\ (1s\ ^2S)\ (5\ ^2\Sigma^+)$ states from bottom to top for both adiabatic and diabatic states.

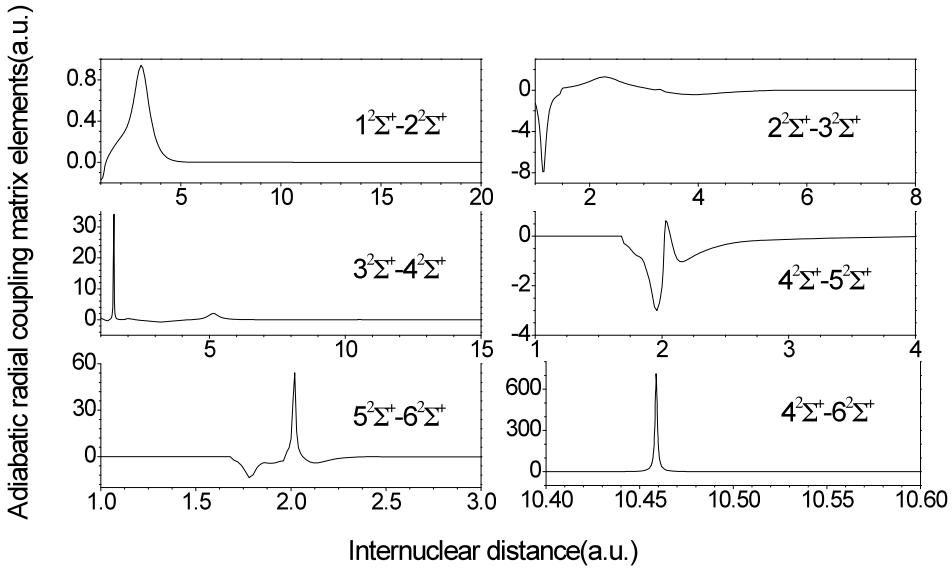

Fig. 2. Adiabatic radial couplings of $[CHe]^{3+}$ as a function of internuclear distance. It should be noted that different scales of height and width are used for the various radial coupling matrix elements.

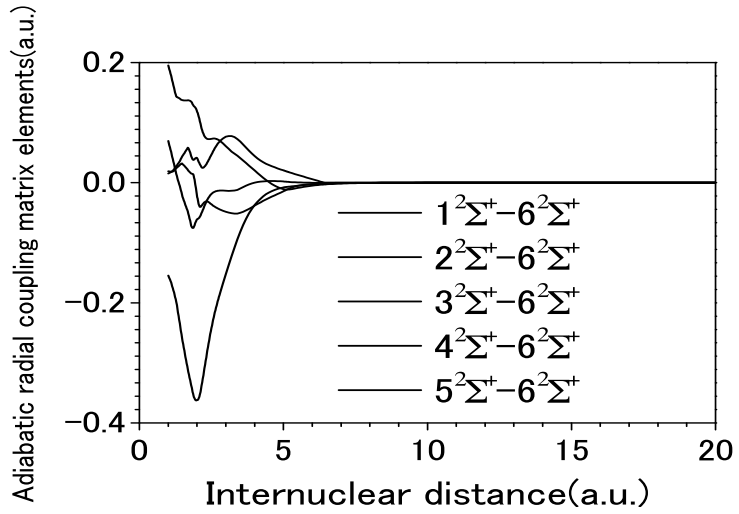

Fig. 3. Diabatic radial coupling of $[CHe]^{3+}$ $^2\Sigma^+$ states as a function of internuclear distance.

B. Total and state-selective cross sections

Using the obtained potential and radial coupling elements with MRDCI approach, the MOCC method has been used to calculate the total and state-selective single-electron capture cross sections for collisions of C^{3+} with He in the energy region from 10^{-4}eV/u to 10^{3}eV/u. The total cross sections are compared with available experimental and theoretical results, as shown in Fig. 4. At the very low energies, the MOCC results display the typical Langevin $E^{-1/2}$ behavior, indicating that the polarization interaction dominates the capture process in this energy region. The total cross section reaches a local minimum near 0.03eV/u, and then increases slowly to a local maximum at about 12eV/u and decreases again to another minimum near 140eV/u. This is somewhat due to the multichannel interference between the different final channels. The same energy dependence behavior is found in the measurements of Ishii et al. [7] for the total charge transfer cross section. For the single-electron capture cross section in the energy region(>5eV/u), the current MOCC calculations agree with the measured data of Ishii et al. [7] and Iwai et al. [4] almost within experimental error, while the results are about 100% larger than the measured data at the lower energies(E <5 eV/u). This difference may be caused by angular scattering effects [30] in the measurements that will tend to underestimate the absolute cross section for very low collision energies. Obvious discrepancies exist for both the trend and the magnitude of the MCLZ calculations of Ishii et al. [7] for collision energies larger than 100eV/u, despite the MCLZ calculations seem to agree better with the measurements of Ishii et al. [7] for collision energies less than 100eV/u. The discrepancies may be related to empirical parameters used in the MCLZ method in which the core excitation is treated approximately with a model potential, and may also be due to the two-channel treatment in the MCLZ model. Especially at the higher energy, contributions from other channels besides the dominant one become important, as will be explained in detail in the following section. Large differences exist for the COB calculations compared with the available experimental results as well, both in trend and magnitude, especially in the lower energies (E <5 eV/u). The double electron capture (DEC) process has been neglected in the present MOCC calculation because of its negligible contributions in the energy region considered in the present work. As discussed above, the first double electron capture channel is an endoergic channel and a large energy interval exists between this channel and the initial one in the asymptotic region, and strong interaction with the initial channel may appear for very short-range avoided crossings which will give important contributions only at very high energy. This has been illustrated by the experiment of Ishii et al. [7], in which the double electron capture (DEC) cross sections only were measured at collision energy

larger than 200eV/u and the DEC cross sections are about four orders of magnitude smaller than the corresponding SEC cross sections. Furthermore, it is very interesting that prominent oscillation structures are found for the total charge transfer cross section in the whole collision energy region. Similar oscillation picture has also be found in our previous work on O^{3+}+He[31]. These oscillation structures will be presented in detail in the state-selective cross section of the next section.

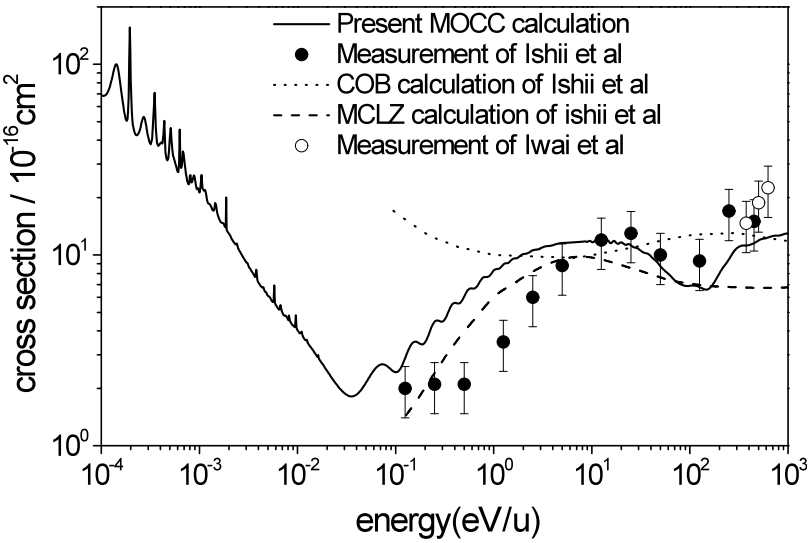

Fig. 4. Total single-electron capture cross sections for C^{3+} + He. Solid line: the present MOCC results for single electron capture (SEC); dotted line: Ishii et al.'s[7] COB results for the SEC process; dashed line: Ishii et al.'s [7] MCLZ results for the SEC process; filled circles: the SEC cross sections of Ishii et al.'s experiment [7] ; unfilled circles: the SEC cross sections of Iwai et al.'s experiment [4].

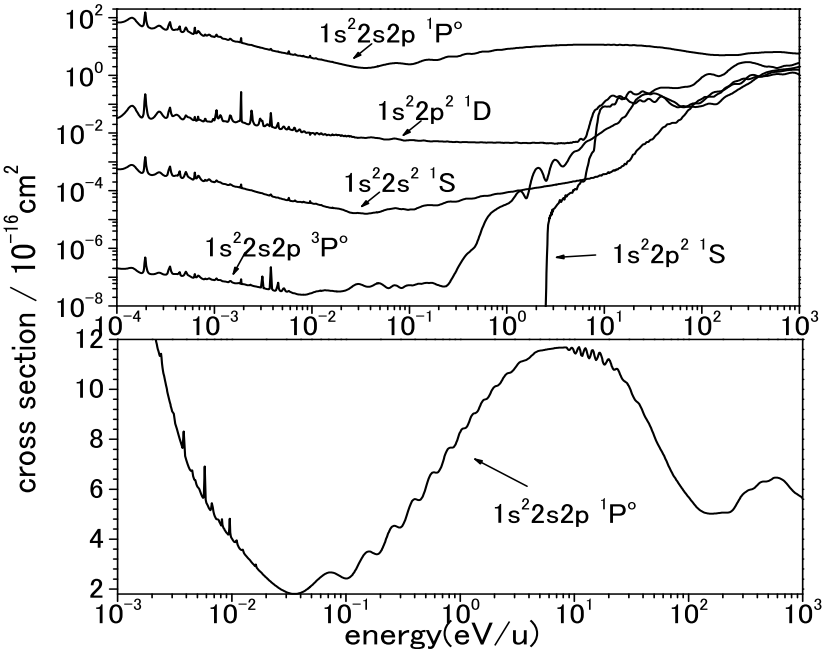

Fig. 5. MOCC calculations of state-selective single-electron capture C^{3+} + He.

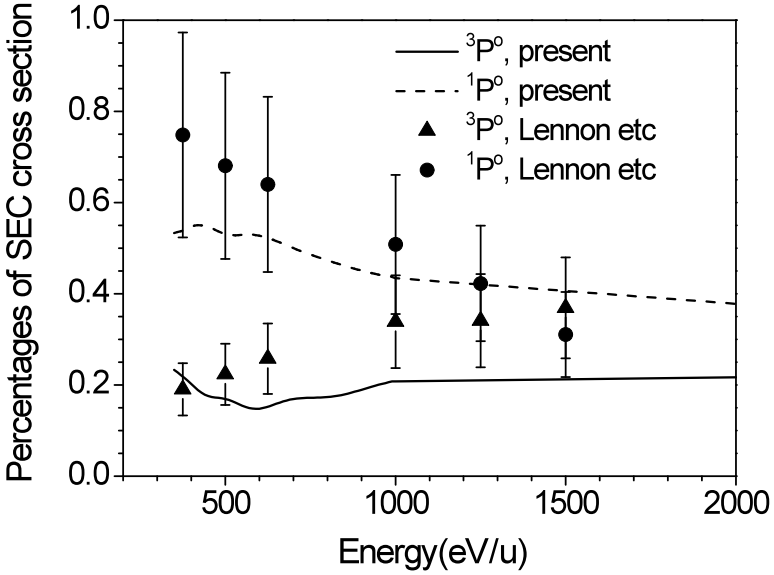

Fig. 6 The state-selective SEC cross section percentage for capture to $C^{2+}(1s^22s2p\ ^3P^o)$ and $C^{2+}(1s^22s2p\ ^3P^o)$ in the total SEC cross section. Dashed line: the present MOCC calculation of the percentage of $C^{2+}(1s^22s2p\ ^1P^o)$ to the total cross section; solid line: the present MOCC calculation of the percentage of $C^{2+}(1s^22s2p\ ^3P^o)$ to the total cross section; the filled circles: Measured value of the percentage of $C^{2+}(1s^22s2p\ ^1P^o)$ to the total cross section of Lennon et al. [5]; the filled triangles: Measured value of the percentage of $C^{2+}(1s^22s2p\ ^3P^o)$ to the total cross section of Lennon et al. [5].

The state-selective single-electron capture cross sections are shown in Fig. 5. The capture to the channel $C^{2+}(1s^22s2p\ ^1P^o)+He^+(1s\ ^2S)$ dominates the charge transfer process in the whole energy region considered, and this is a consequence of the avoided crossing with much broader and smaller radial coupling at R≈5.2 a_0 between 3 $^2\Sigma^+$ and 4 $^2\Sigma^+$. However, with increasing energy, the cross sections for capture to $C^{2+}(1s^22s2p\ ^1P^o)+He^+(1s\ ^2S)$ keeps almost constant and the ones to other four channels $C^{2+}(1s^22s^2\ ^1S)+He^+(1s\ ^2S)$, $C^{2+}(1s^22s2p\ ^3P^o)+He^+(1s\ ^2S)$, $C^{2+}(1s^22p^2\ ^1D)+He^+(1s\ ^2S)$ and $C^{2+}(1s^22p^2\ ^1S)+He^+(1s\ ^2S)$ increase rapidly with collision energy larger than 6eV/u. As the incident energy increases above 100eV/u, the cross sections for capture to other channels become comparable in magnitude with the one to $C^{2+}(1s^22s2p\ ^1P^o)+He^+(1s\ ^2S)$, which is due to those short-range avoided crossings. Therefore, at higher collision energies, the multichannel interaction effect becomes more important and more states should be included in the MOCC calculation，which may explain the discrepancies between the MCLZ calculation of Ishii et al. and their measurements at higher energies, because the MCLZ is a two-channel model essentially. At higher energy above 1keV/u, the contributions from the endergonic channels will be not negligible and the DEC process should be considered as well. Experimentally, Lennon et al. [5] have only reported state-selective cross sections data at a few collision energies (see Table 5. of ref. [5]) and their results have been normalized to the total one-electron capture cross section obtained by Iwai et al. [4]. At these collision energies points, the most important two channels are $C^{2+}(1s^22s2p\ ^1P^o)+He^+(1s\ ^2S)$ and $C^{2+}(1s^22s2p\ ^3P^o)+He^+(1s\ ^2S)$. For comparison, the cross section percentage of these two channels to the total cross sections are computed and shown in Fig 6 with the results of Ref. 13. It can be found that the present calculations generally agree with the measurements of Lennon et al. [5], especially for the dominant channel of $C^{2+}(1s^22s2p\ ^1P^o)+He^+(1s\ ^2S)$. Remarkable oscillation structures are present in the whole collision energy region considered in the present work for the individual state-selective cross

section. The sharp, narrow structures at energies mostly below 0.01eV/u may be the shape resonances, the mild structures below 0.02eV/u approximately may be the Regge oscillations, caused by the Regge poles and the third type of oscillation in higher energies, extended to a few 10eV/u may be the glory oscillations. All three types of oscillations will be superimposed on each other. Such structures have been found by Krstic et al. [32] in the elastic scattering cross sections for H^+ + H and H^+ with inert gases. Detailed analysis of these oscillation structures will be given systematically with the similar structures found in another system of O^{3+}+He in an upcoming paper.

C. Total and state-selective rate coefficients

Using the MOCC cross sections, we computed the total and state-selective rate coefficients as displayed in Fig. 7 and collected in Table 2. Compared to the calculations of Butler and Dalgarno [8] for a few energy points, the present MOCC data are one to two orders of magnitude larger than their results in the temperatures from 10^3 K to$10^{4.5}$ K. The large discrepancy may be due to the unsuccessful description of charge transfer process for the system with complex reaction channels. As discussed above, the discrepancy is related to the approximate treatment of core excitation, but probably also to our multichannel treatment. It can be found from Fig. 7(b) that the rate coefficients for capture to $C^{2+}(1s^22s2p\ ^1P^o)$ dominate over other channels in the whole temperature range considered. With increasing temperature of *T*, the rate coefficients for capture to other states increase rapidly, which become comparable with the capture to the $C^{2+}(1s^22s2p\ ^1P^o)$ at $T = 10^6$ K, especially for capture to states of $C^{2+}(1s^22s2p\ ^3P^o)$ and $C^{2+}(1s^22p^2\ ^1S)$.

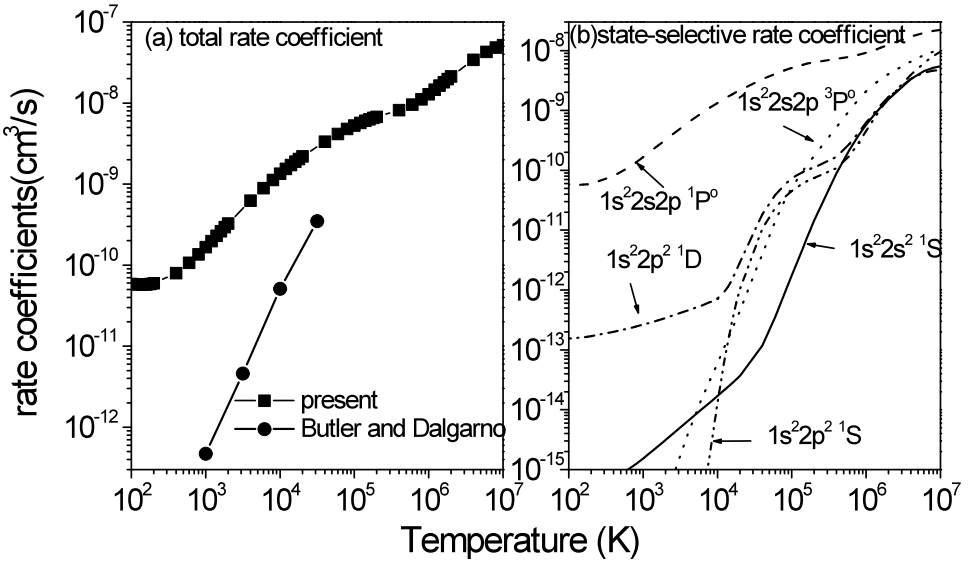

Fig. 7 Total and state-selective rate coefficients in charge transfer of $O^{3+}(^2P^o)$ with He as a function of temperature. (a) Total rate coefficients: Solid line with filled squares: present results; Solid line with filled circles: results of Butler and Dalgarno [8]; (b) State-selective rate coefficients: line.

Table 2. Total and state-selective charge transfer rate coefficients (cm^3/s) as a function of temperature.

T(k)	Total	$^1S(1s^22s^2)$	$^3P^o(1s^22s2p)$	$^1P^o(1s^22s2p)$	$^1D(1s^22p^2)$	$^1S(1s^22p^2)$
100	5.87E-11	5.15E-16	5.90E-19	5.86E-11	1.55E-13	
120	5.78E-11	5.06E-16	6.67E-19	5.76E-11	1.57E-13	
140	5.75E-11	5.04E-16	7.42E-19	5.73E-11	1.60E-13	
160	5.78E-11	5.08E-16	8.14E-19	5.77E-11	1.63E-13	
180	5.86E-11	5.15E-16	8.83E-19	5.84E-11	1.67E-13	
200	5.96E-11	5.25E-16	9.47E-19	5.95E-11	1.70E-13	
400	7.99E-11	7.12E-16	1.51E-18	7.97E-11	1.99E-13	
600	1.07E-10	9.61E-16	2.54E-18	1.07E-10	2.23E-13	
800	1.36E-10	1.24E-15	6.43E-18	1.36E-10	2.45E-13	
1000	1.67E-10	1.53E-15	1.77E-17	1.67E-10	2.64E-13	
1200	1.98E-10	1.84E-15	4.13E-17	1.98E-10	2.81E-13	8.35E-25
1400	2.30E-10	2.15E-15	8.17E-17	2.30E-10	2.97E-13	1.915E-23
1600	2.62E-10	2.47E-15	1.42E-16	2.62E-10	3.13E-13	2.33E-22
1800	2.94E-10	2.80E-15	2.26E-16	2.94E-10	3.27E-13	1.69E-21
2000	3.26E-10	3.12E-15	3.38E-16	3.25E-10	3.41E-13	8.41E-21
4000	6.25E-10	6.49E-15	3.99E-15	6.25E-10	4.55E-13	1.36E-17
6000	8.90E-10	9.93E-15	1.42E-14	8.90E-10	5.46E-13	2.22E-16
8000	1.13E-9	1.34E-14	3.23E-14	1.13E-9	6.27E-13	2.01E-15
10000	1.34E-9	1.70E-14	6.05E-14	1.34E-9	7.27E-13	1.31E-14
12000	1.54E-9	2.06E-14	1.02E-13	1.54E-9	8.87E-13	5.29E-14
14000	1.72E-9	2.44E-14	1.58E-13	1.72E-9	1.15E-12	1.50E-13
16000	1.89E-9	2.83E-14	2.32E-13	1.89E-9	1.57E-12	3.32E-13
18000	2.04E-9	3.24E-14	3.27E-13	2.04E-9	2.16E-12	6.22E-13
20000	2.19E-9	3.67E-14	4.46E-13	2.19E-9	2.94E-12	1.03E-12
40000	3.35E-9	1.18E-13	4.02E-12	3.31E-9	1.85E-11	1.06E-11
60000	4.16E-9	3.57E-13	1.43E-11	4.09E-9	3.89E-11	2.35E-11
80000	4.79E-9	8.68E-13	3.07E-11	4.67E-9	5.75E-11	3.53E-11
100000	5.29E-9	1.74E-12	5.09E-11	5.12E-9	7.26E-11	4.52E-11
120000	5.70E-9	3.07E-12	7.31E-11	5.48E-9	8.44E-11	5.34E-11
140000	6.03E-9	4.94E-12	9.65E-11	5.78E-9	9.34E-11	6.01E-11
160000	6.31E-9	7.43E-12	1.21E-10	6.02E-9	1.00E-10	6.56E-11
180000	6.55E-9	1.06E-11	1.47E-10	6.22E-9	1.06E-10	7.02E-11
200000	6.76E-9	1.44E-11	1.74E-10	6.39E-9	1.11E-10	7.42E-11
400000	8.19E-9	8.93E-11	5.25E-10	7.30E-9	1.68E-10	1.09E-10
600000	9.56E-9	2.23E-10	1.01E-9	7.87E-9	2.79E-10	1.75E-10
800000	1.12E-8	3.91E-10	1.55E-9	8.49E-9	4.37E-10	2.90E-10
1000000	1.29E-8	5.76E-10	2.08E-9	9.15E-9	6.23E-10	4.51E-10

IV. CONCLUSION

In the present work, charge transfer processes due to collisions of ground state $C^{3+}(1s^22s\ ^2S)$ ions with atomic helium are investigated using the quantum-mechanical molecular-orbital close-coupling (MOCC)

method. The *ab initio* adiabatic potential and radial coupling utilized in the QMOCC calculations are obtained from the MRD-CI approach. Total and state-selective single electron capture (SEC) cross sections and rate coefficients are provided for collision energies from 10^{-4}eV/u to 10^{3}eV/u and from 10^{2}K to 10^{6}K, respectively. Comparison with existing data shows that the present MOCC calculations agree well with the experimental results for total single-electron capture cross sections. As for the discrepancy that appears in the low-energy region, it may be due to the angular scattering effects in the measurements that will tend to underestimate the absolute cross section for very low collision energies. Further theoretical and experimental studies are needed to validate the current work in this regard. The Landau–Zener calculations of the total SEC rate coefficient of Butler and Dalgarno [8] are one or two orders of magnitude smaller than the present results in the temperature region from 10^{3} K to$10^{4.5}$ K. Therefore, *ab initio* quantal calculation is necessary for precise description of the charge transfer processes for such systems with complex reaction channels.

ACKNOWLEDGEMENTS

The author would like to thank Professor P S Krstic for helpful discussions. This work was partly supported by the National Natural Science Foundation of China (Grant No.s 10604011, 10734140，10008803 and 10878008) and the National Key Laboratory of Computational Physics Foundation (No.9140C6904030808). Y. Wu would also like to acknowledge support from the JSPS-China core-university program.

[1] S. Lepp and R. McCray, Astrophys. J. 269, 560 (1983).

[2] S. I. Krasheninnikov, A. Yu. Pgarov and D. J. Sigmar, Phys. Lett. A 214, 295 (1996); ibid, A 222, 251 (1996).

[3] R. K. Janev, T. Kato and J. G. Wang, Phys. Plasma 7, 4364 (2000).

[4]T Iwai, Y Kaneko, M Kimura, N Kobayashi, S Ohtani, K Okuno, S Takagi, H Tawara and S Tsurubuchi, Phys. Rev. A **26**, 105(1982)

[5] M Lennon, R W McCullough and H B Gilbody, J. Phys. B **16**, 2191 (1983)

[6] M Kimura, T Iwai, Y Kaneko, N Kobayashi, A Matsumoto, S Ohtani, K Okuno, S Takagi, H Tawara and S Tsurubuchi, J. Phys. B **15**, L851 (1982)

[7] K. Ishii, A. Itoh and K. Okuno, Phys. Rev. A **70** 042716 (2004)

[8] Butler S E and Dalgarno A, strophys. J., Part 1 241, 838(1980)

[9] R. J. Buenker, and S. D. Peyerimhoff, Theoret. Chim. Acta 35, 33 (1974); 39, 217 (1975); R. J. Buenker Int. J. Quantum Chem. 29,435 (1986).

[10] R. J. Buenker, in Proceedings of the Workshop on Quantum Chemistry and Molecular Physics, Wollongong, Australia, edited by P. G. Burton (Wollongong University Press, Wollongong, Autsralia, (1980); in Study in Physical and Theoretical Chemistry, edited by R. Carbo, Current Aspects of Quantum Chemistry Vol. 21(Elsvier, Amsterdam, 1981), p.17; R. J. Buenker and R.A.Phillips,J.Mol.Struc.: THEOCHEM 123, 291 (1985).

[11] S. Krebs, and R. J. Buenker, J. Chem. Phys. 103, 5613 (1995).

[12] D.E. Woon and T.H. Dunning, Jr. J. Chem. Phys. 100, 2975 (1994)

[13] T.H. Dunning, Jr. J. Chem. Phys. 90, 1007 (1989).

[14] http://physics.nist.gov/cgi-bin/ASD/energy1.pl

[15] B. Herrero, I. L. Cooper and A. S. Dickinson, J. Phys. B: At. Mol. Opt. Phys. 29, 5583 (1996).

[16] G. Hirsch, P. J. Bruna, R. J. Buenker, and S. D. Peyerimhoff, Chem. Phys. 45, 35 (1980).

[17] http://physics.nist.gov/cgi-bin/ASD/energy1.pl; W. L. Wiese, J. R. Fuhr and T. M.Deters, J. Phys.

Chem. Ref. Data, Monograph No. 7 (1996); G. W. F. Drake and W. C. Martin, Can. J. Phys. **76** 679 (1998)

[18] M. Kimura and N. F. Lane, Ad. At. Mol. Phys. 26, 79 (1990).

[19] B. Zygelman, D. L. Cooper, M. J. Ford et al., Phys. Rev. A 46, 3846 (1992).

[20] J. G. Wang et al., Phys. Rev. A 67, 012710 (2003); Phys. Rev. A 69, 062703 (2004).

[21] B. R. Johnson, J. Comp. Phys. 13, 445 (1973).

[22] T. G. Heil, S. E. Butler and A. Dalgarno, Phys. Rev. A 27, 2365 (1983).

[23] D. L. Cooper, N. J. Clarke, P. C. Stancil and B. Zygelman, Adv. Quant. Chem. 40, 37 (2001).

[24] B. H. Brandsen and M. R. C. McDowell, Charge Exchange and the Theory of Ion-Atom Collisions (Clarendon Press, Oxford, 1992).

[25] A. R. Turner, D. L. Cooper, J. G. Wang, and P. C. Stancil, Phys. Rev. A 68, 012704 (2003).

[26] P. C. Stancil et al., J. Phys. B: At. Mol. Opt. Phys. 34, 2481 (2001).

[27] J. G. Wang et al., J. Phys. B: At. Mol. Opt. Phys. 35, 3137 (2002).

[28] R. K. Janev, L. P. Presnyakov, and V. P. Shevelko, *Physics of Highly Charged Ions,* Springer-Verlag, New York, 1985.

[29] L. F. Errea, C. Harel, H. Jouin, L. Méndez, B. Pons, and A. Riera, J. Phys. B 27, 3603 (1994).

[30] Nielsen, E. H., Andersen, L. H., Barany, **A.,** Cederquist, H., Heinemeier, J., Hvelplund, P., Knudsen, H., MacAdam, K. B. and Ssrensen, J., J. Phys. **B18,** 1789 (1985).

[31] Y. Wu, Y.Y.Qi, S.Y.Zou, J. G. Wang, Y. Li, R. J. Buenker and P. C. Stancil (to be submitted)

[32] P. S. Krstic, J. H. Macek, S. Yu. Ovchinnikov, and D. R. Schultz, Phys. Rev. A **70**, 042711 (2004); J. H. Macek, P. S. Krstic, and S. Yu. Ovchinnikov, Phys. Rev.Lett. **93**, 183203(2004); S. Yu. Ovchinnikov, P. S. Krstic, and J. H. Macek, Phys. Rev. A **74**, 042706 (2006)